Hindawi
International Journal of Photoenergy
Volume 2023, Article ID 5442031, 12 pages
https://doi.org/10.1155/2023/5442031

Research Article

Numerical Study of High Spectral Efficiency and High-Temperature Energy Harvesting Metamaterial Emitter to Improve Thermophotovoltaic Performance

Sifan Tamiru, Fekadu Tolessa, Birke Alemu, Solomon Tiruneh, Abebe Belay, Gurmu Alemu, and T. Gurumurthi

Department of Applied Physics, School of Applied Natural Science, Adama Science and Technology University, Adama, Ethiopia

Correspondence should be addressed to Fekadu Tolessa; tolasaa21@gmail.com

Received 6 March 2023; Revised 30 June 2023; Accepted 17 August 2023; Published 7 September 2023

Academic Editor: Qiliang Wang

Design work was done on a broadband and wide-angle selective pyramid metamaterial emitter. COMSOL Multiphysics software was used to study the emitter, which was made of tungsten and aluminum nitride. The width of the unit cell and the tungsten ground thickness were fixed while other geometric parameters, such as the base length of the pyramid, the height of the pyramid, and the thickness of the dielectric, were tuned to produce the emitter's desired broadband emission. A high average emissivity over 0.96 below the cutoff wavelength (0.1 μm-2.2 μm) was seen in the numerical simulation. The developed metamaterial emitter also had good emissivity across a broad range of incidence angles, from 0° to 60°, and was polarization independent. In addition, the planned emitter for the InGaAs cell has a better spectral efficiency than the blackbody *other designed emitter*. In general, the planned selective nanopyramid emitter was realized with 75% spectrum efficiency for InGaAs band gap energy (0.55 eV) at 1200 K, which was greater than blackbody and prior papers.

1. Introduction

A thermophotovoltaic system produces more power since it is designed for various temperature ranges and has a high capacity to absorb numerous quantities of energy at maximum theoretical efficiency [1, 2]. An emitter, a heat source, and a TPV cell are the basic components of a TPV system [3]. Photons are produced by heat sources such as solar, burning fossil fuels, and waste energy [4]. Emitters are devices that convert the photon from a heat source to thermal radiation [5]. The heat radiation is collected by the TPV cell, a semiconductor that may produce electron-hole pairs and subsequently photocurrent. When the photon energy is greater than the TPV cell's energy band gap, electromagnetic energy can only be converted to electrical power [5–8]. The basic problems with TPV systems are low conversion efficiency and power generation [9]. To improve conversion efficiency and power generation, the emitter must have the highest possible emittance within a range of cutoff wavelengths that fits a specific TPV cell and the lowest possible emittance outside of the cutoff wavelength [10].

As stated before, the efficiency of the TPV system depends on the emitter, which can be controlled by both the choice of material and the emitter design. Emitters are designed from different materials, such as polycrystalline silicon carbide [11], tungsten [12], rare-earth oxides [13], photonic crystals [14], and metamaterials. However, in order to improve emitter efficiency, power generation, and performance of TPV cell metamaterials, one must be more selective. Metamaterials (MM) are man-made materials with unique features such as repeating patterns on microscopic scales that do not exist in nature. They are made up of numerous components comprised of composite materials, including metals and polymers. The materials are frequently organized in repeating patterns that are smaller in size than the wavelengths of the phenomena they affect [15]. The characteristics of MM are derived from their uniquely

developed structures, not from the qualities of the underlying materials. Their exact shape, geometry, size, orientation, and arrangement confer on them the ability to influence electromagnetic waves [16]. They are used for a variety of purposes, one of which is as an absorber.

Landy et al. proposed the first MM absorber, which is a narrow band absorber based on metal–insulator–metal (MIM) [17]. Many academics have constructed many types of MM absorbers after Landy et al. for attaining single band or multiband absorption, but most scholars have recently shown a strong interest in ultraband absorption. Scholars primarily postulated and demonstrated that metal nanostructures extended the absorber's absorption spectrum. According to the Kirchhoff law, the absorber produced from a metal nanostructure is employed as a broadband absorber that is used as a metamaterial emitter [18]. To improve TPV performance, MM emitters are often built with diverse symmetry shapes such as disks [19], squares [6], crosses [20], pyramids [21], cones [22], and multilayers [23, 24]. Recently, metamaterial emitters have been developed to increase the effectiveness of TPV systems. Wang et al. [21] design a metamaterial-selective solar absorber with titanium nanostructured gratings deposited on an ultrathin MgF2 spacer and tungsten ground film. This solar absorber normal absorptance is higher than 90% in the UV, visible, and near-infrared (IR) regimes, while the mid-IR emittance is around 20%. Also, Song et al. [25] achieve emissivity 0.953 between 600 and 1800 nm by designing a 2D trilayer grating using a tungsten/silica/tungsten ($W/SiO_2//W$) structure on a tungsten substrate. Additionally, a funnel-shaped anisotropic metamaterial absorber is reported with a periodic array of nickel–germanium (Ni/Ge) which achieves 96% absorption through wavelength 200 nm to 900 nm designed by Abdelatif et al. [26]. Maremi et al. [23] have also designed a multilayer nanoring emitter for an InGaAs band gap of 0.6 eV and obtain 79.6% spectral efficiency at 1400 K. Furthermore, the multilayer ring metamaterial (MTM) emitter with a cutoff wavelength of 2.34 μm that achieves a spectral efficiency of 85.6% for the InGaAsSb cell at 1600 K is designed by Jiang et al. [24].

For the band gap of InGaAs, the TPV system's efficiency and power output were improved in this work by the use of a metamaterial emitter. The characteristics of the planned nanopyramid structure, such as the base length (b_1), height of pyramid (h_1), and dielectric thickness (h_2), were optimized based on numerical modeling by using COMSOL Multiphysics. Near-perfect and wide-angle emissivity was achieved at the desired wavelength, with a cutoff wavelength of 2.2 μm. The obtained emissivity range is also greater than that reported by Wang et al. [21], Song et al. [25], Abdelatif et al. [26], Maremi et al. [23], Jiang et al. [24], and Abdel-Latif et al. [7]. The developed emitter has a simple design and is easy to fabricate from Maremi et al. [23], Jiang et al. [24], and Abdel-Latif et al. [7] and also achieve high efficiency when compared to the blackbody and earlier prototype MM emitters; the developed metamaterial emitter achieved a spectral efficiency of 75% at 1200 K.

2. Method and Materials

2.1. Numerical Simulation. Figure 1 shows a MM emitter made of tungsten and aluminum nitride (AlN) subjected to harmonic excitation at one or more wavelengths. It was used to calculate the structure's transmission and reflection versus wavelength in electromagnetic wave propagation through the designed structure.

The design specifications included W (width of unit cell), h_1 (top tungsten height), h_2 (dielectric thickness), h_3 (ground tungsten thickness), b_1 (base length of pyramid), and a ratio of 0.5 from the base to the top of the pyramid. W is chosen because of its high melting temperatures of around 3695 K and strong corrosion resistance [7]. AlN is also chosen because of their high melting point of about 2345 K. A metal-dielectric-metal structure, or a nanopyramid that begins and ends with the letter W, was created. An electromagnetic wave that strikes a plane may be absorbed, reflected, or transmitted. The absorption is calculated as

$$A = 1 - R - T = 1 - (s_{11})^2 - (s_{21})^2, \tag{1}$$

where A is the absorptivity, R is the reflectivity, T is the transmittance, s_{11} is the reflection coefficient, and s_{21} is the transmission coefficient. The transmittance of the W film is zero ($T = 0$) because the skin depth of the W film is less than 100 nm [24, 27], and a midinfrared electromagnetic wave cannot travel through the W film. Therefore, the absorption can be expressed as

$$A = 1 - R = 1 - (s_{11})^2. \tag{2}$$

The absorptivity (A) and emissivity (ε) are derived by using Kirchhoff's law, which stipulates that the higher the absorptivity, the higher the emissivity. With the assumption of no transmittance, an object's emissivity is equal to its absorptivity for a given frequency, polarization, and direction:

$$\varepsilon(\lambda) = A(\lambda) = 1 - R = 1 - (s_{11})^2. \tag{3}$$

For a material to be a perfect absorber, there must be little to no transmission and reflection of impinging light. Reflection is reduced when the impedance of the materials and the impedance of the surrounding environment are equal. Lastly, the simulation results were applied to determine the emissivity based on absorptivity.

3. Results and Discussion

3.1. Effect of Base Length of Pyramid. To modify the electromagnetic properties, adjust the W and AlN parameters, such as the base length, height, and dielectric thickness. The constructed emitter's emissivity and reflectivity are shown in Figures 2(a) and 2(b), respectively, when b_1 was increased from 95 nm to 295 nm. As seen in the picture, the emitter's reflectivity changed as b_1 changed but in the opposite direction from how it changed in terms of emissivity. The

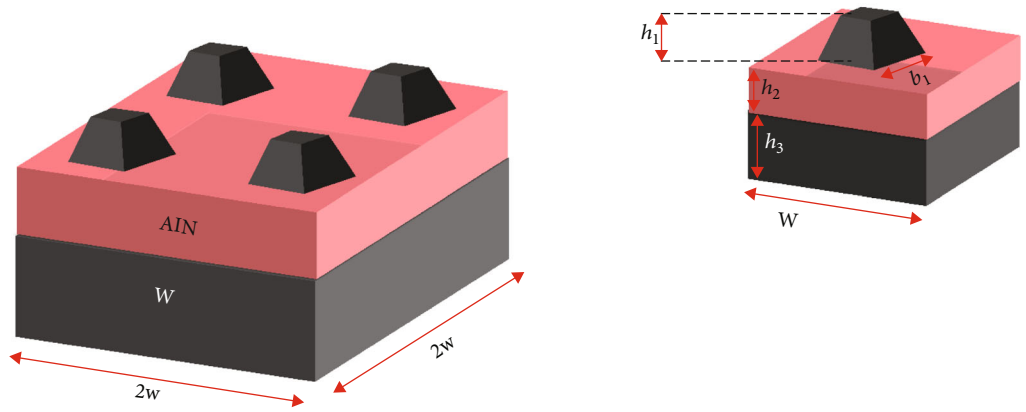

Figure 1: Schematic representation of the designed metamaterial structure and unit cell of the reported nanopyramid.

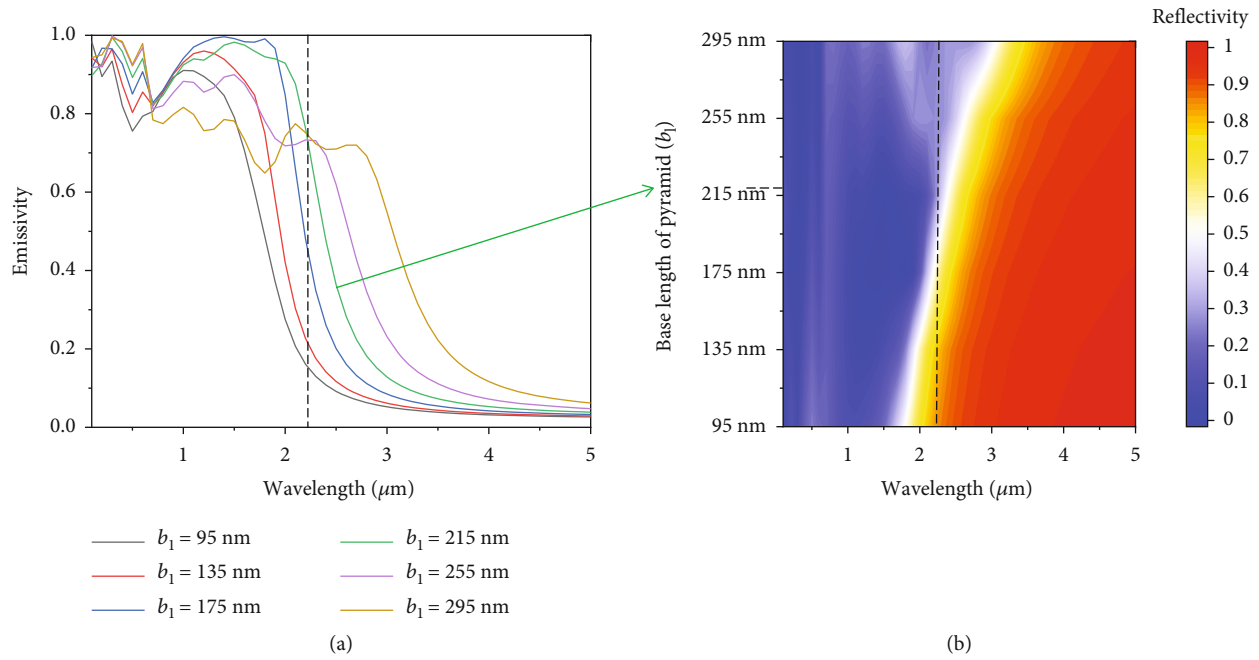

Figure 2: The effect of base length of pyramid (b_1) on the spectra (a) emissivity and (b) reflectivity of proposed nanopyramid metamaterial with h_1 = 120 nm and h_2 = 115 nm.

reflectivity before the cutoff wavelength reduced, and the emissivity improved when b_1 was increased from 95 nm to 215 nm; however, the reflectivity of the emitter increased somewhat when b_1 was increased from 215 nm to 295 nm. This result indicated that the pyramid's length had an impact on the emitter's electromagnetic characteristic.

In order to explain the perfect broadband absorption, the electromagnetic environment around the nanopyramid emitter was looked at. The high inherent loss of tungsten as a result of design was highlighted as a metal-dielectric-metal (MDM) structure, and the combination of these resonances boosted broadband emissivity. Various excitation processes happened with resonance frequencies such as MPs and SPP [23]. Between the ground film layer and the first W layer, as well as between two subsequent metal (W) layers, the AlN layer was placed. MP is the excitation technique that can effectively localize the electromagnetic energy in these layers (metal-dielectric-metal, or W-AlN-W). Free charge caused a net flow of oscillating electric currents on the thin film W surfaces of the ground layer, the first W layer, or between two sublayers in the nanopyramid, which produced induced magnetic fields [28]. A nearly perfect broadband emissivity was produced by the simultaneous cooperation of magnetic polariton resonances at a certain wavelength.

SPP caused the first peak on the graph in Figure 2(a), while MP caused the second peak, according to the simulation's findings. MP is pushed to the longer wavelength by b_1, as can be seen on the graph in Figure 2(a), where the change of b_1 had a considerable influence on MP and a minor one on SPP. When the cutoff wavelength was taken into account, the broadest and most nearly perfect broadband emissivity occurred at b_1 = 215 nm (green line), h_1 = 120 nm, and h_2 = 115 nm.

3.2. Effect of Pyramid Height. Figure 3 shows how the emissivity and reflectivity of metamaterial vary with the height of the pyramid when the pyramid's base length and the dielectric thickness are constant at 215 nm and 115 nm, respectively. The impact of adjusting h_1 from 40 nm to 240 nm on the reflectivity and emissivity of the planned emitter is seen in Figures 3(a) and 3(b). The simulation results show that the average emissivity increased while the average reflectivity decreased when h_1 was optimized from 40 nm to 160 nm before the cutoff wavelength (<2.2 μm), and the average emissivity decreased while the average reflectivity increased when h_1 was optimized above the cutoff wavelength (>2.2 μm). The average emissivity reduced marginally, and the average reflectivity increased slightly prior to the cutoff wavelength when h_1 was raised from 160 nm to 240 nm. At $h_1 = 160$ nm (green line), $b_1 = 215$ nm, and $h_2 = 115$ nm, the emitter attained broadband emissivity spanning the wavelength range of 0.1 μm to 2.2 μm.

3.3. Effect of Dielectric Thickness. The dielectric thickness of the spaces between metalized regions on an MM emitter plays a key role in determining the device's resonant frequency. Two metal regions near to one another will create capacitance, which will further alter the induced fields. As the distance between the metal regions is changed, the capacitance and therefore the resonant frequency will fluctuate. The resonance frequency changes somewhat as the gap width expands. Figures 4(a) and 4(b) illustrate how emitter emissivity and reflectivity are affected by dielectric thickness at constant pyramid h_1 and b_1.

The emissivity and reflectivity of the planned emitter changed as the dielectric thickness increased in Figures 4(a) and 4(b), from 45 nm to 220 nm, respectively. The simulation results show that the average emissivity increased and the average reflectivity decreased when h_2 was optimized from 45 nm to 80 nm before the cutoff wavelength (<2.2 μm), whereas the average emissivity decreased and the average reflectivity increased when h_2 was optimized above the cutoff wavelength (>2.2 μm). Before the cutoff wavelength, the average of the emissivity fell and the average of the reflectivity rose as h_2 grew from 80 nm to 220 nm. At $h_2 = 80$ nm (red line), $b_1 = 215$ nm, and $h_1 = 160$ nm, the emitter attained broadband emissivity spanning the wavelength range of 0.1 μm to 2.2 μm.

3.4. Angular Emissivity. Figures 5(a) and 5(b) describe the effects of incidence angles and polarizations on the spectrum emissivity of the produced selective metamaterial emitter with optimal geometric parameters $h_1 = 160$ nm, $h_2 = 80$ nm, and $b_1 = 215$ nm. Figure 5(a) makes the incidence angle 0°, but the outcome shows that the intended metamaterial emitter is polarization angle independent. This explains why the emitter's symmetry was intentional. The outcome shown in Figures 5(b) and 5(c) showed that the emittance curve relatively unchanged when the incidence angle rose from 0° to 60° for TM (transverse magnetic field) and from 0° to 45° for TE (transverse electric field). The emissivity fell marginally when the incidence angle was adjusted to 75° for both TE and TM, but the emittance remained high for TM and very low for TE. This explains that if the magnetic field is parallel to incidence, the emissivity of the emitter falls as the angle of incidence increases. But the incident angle has little effect on TM. This finding demonstrates that the emitter can handle plane waves with a wide range of incidence angles, from 0° to 60° for TM.

3.5. Performance of TPV. Figure 6(a) presents the emission, reflection, and transmission spectra of the optimized emitter at $b_1 = 215$ nm, $h_1 = 160$ nm, $h_2 = 80$ nm, $h_3 = 260$ nm, and $w = 395$ nm. As shown in Figure 6(a), the transmission of the designed emitter was zero. AlN's capacity to block transmission and ground W reflection was responsible for this. The designed emitter was reflected nearly zero before the 2.2 μm and high above 2.2 μm due to the high intrinsic loss of tungsten and coupling of MP and SPP resonance modes [7]. The built-in emitter attained a high emissivity of around 96.4% before 2.2 μm (the shaded area) and a low emissivity above 2.2 μm. The emissivity above 4 nm is shown in Figure 6(b) at $b_1 = 215$ nm, $h_1 = 160$ nm, $h_2 = 80$ nm, $h_3 = 260$ nm, and $w = 395$ nm. The graph shows that the emissivity of the desired MM decreased noticeably as wavelength increased and was less than 5% above 4 nm. As a result, the emitter's spectral efficiency was improved.

Figure 7(a) displays the spectrum emissivity of a proposed TPV emitter at $b_1 = 215$ nm, $h_1 = 160$ nm, $h_2 = 80$ nm, $h_3 = 260$ nm, and $w = 395$ nm with and without a nanopyramid. Due to the excitation of SPP between AlN and bottom W, the first peak was obtained at a short wavelength of 0.2 μm, as can be seen from the peak in Figure 7(a). The MP was able to identify an extra peak at long wavelength $\lambda = 2$ μm due to the interaction between magnetic resonance inside the nanopyramid and the incident electromagnetic radiation through the port. When the emitter was built without a nanopyramid or simply from bottom W and AlN, the emissivity in the shaded area was lowered, and the peaks were formed at 0.1 μm and 0.7 μm due to SPP. As soon as the nanopyramid, or W-AlN-W, was incorporated into the design, the emissivity in the shaded area increased, the first peak expanded and shifted to the longer wavelength, and the second peak enlarged. Due to MP being activated by the interaction between the bottom tungsten and the diamagnetic response inside the nanopyramid, high emissivity was also reached using the suggested configuration [25].

This investigation found that the suggested TPV emitter operated as shown in Figures 7(b) and 7(c) while employing various materials. Figure 7(b) illustrates how metals like Al, Mo, and W affect the dielectric material AlN. Al has weak emissivity throughout a large wavelength range, from 0.1 μm to 2.2 μm, according to its emissivity spectra. Aluminum metal has significant losses in the visible and near-IR wavelengths. Due to Al's substantial actual permittivity value being significantly negative, it was unable to change its optical properties [7]. In contrast, the Mo had poor emissivity in the dark region (before the cutoff wavelength). The developed TPV emitter with AlN/W has a much higher emissivity within the wavelength range under consideration. Figure 7(c) shows how several dielectric materials, including Al_2O_3, SiO_2, and AlN, are affected by the proposed

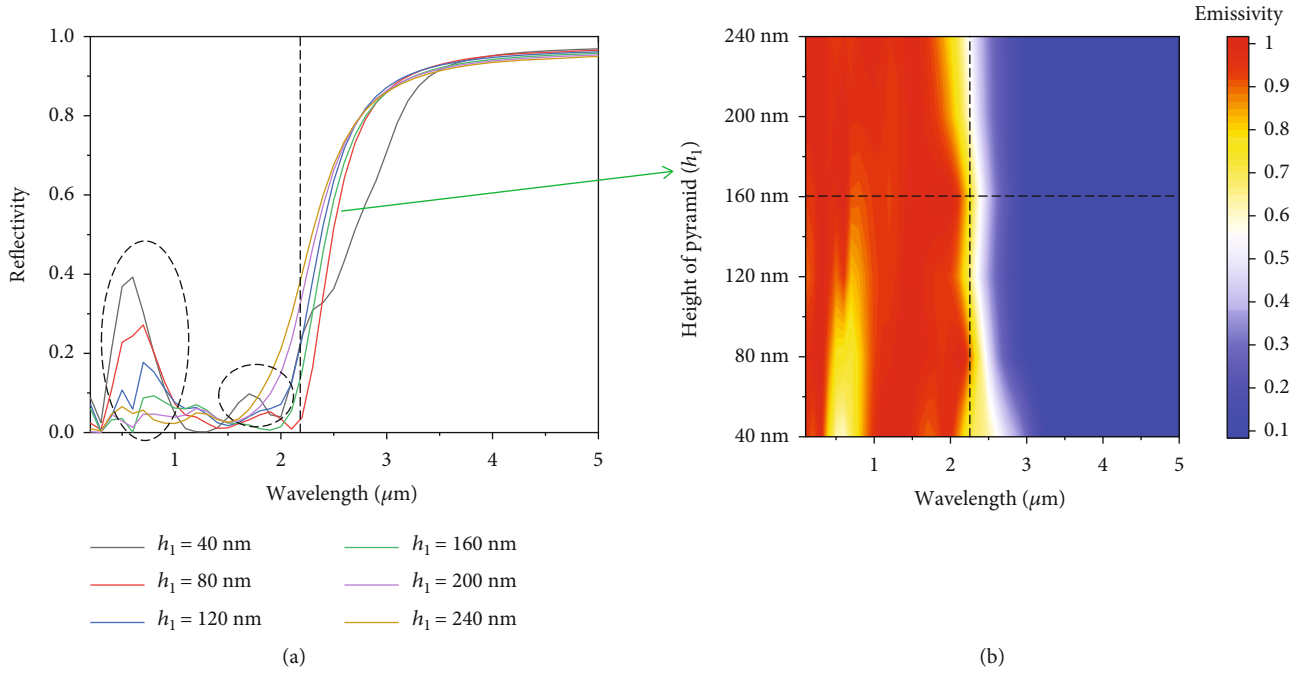

FIGURE 3: The effect of pyramid height (h_1) on the spectral (a) reflectivity and (b) emissivity of designed nanopyramid metamaterial with $b_1 = 215$ nm and $h_2 = 115$ nm.

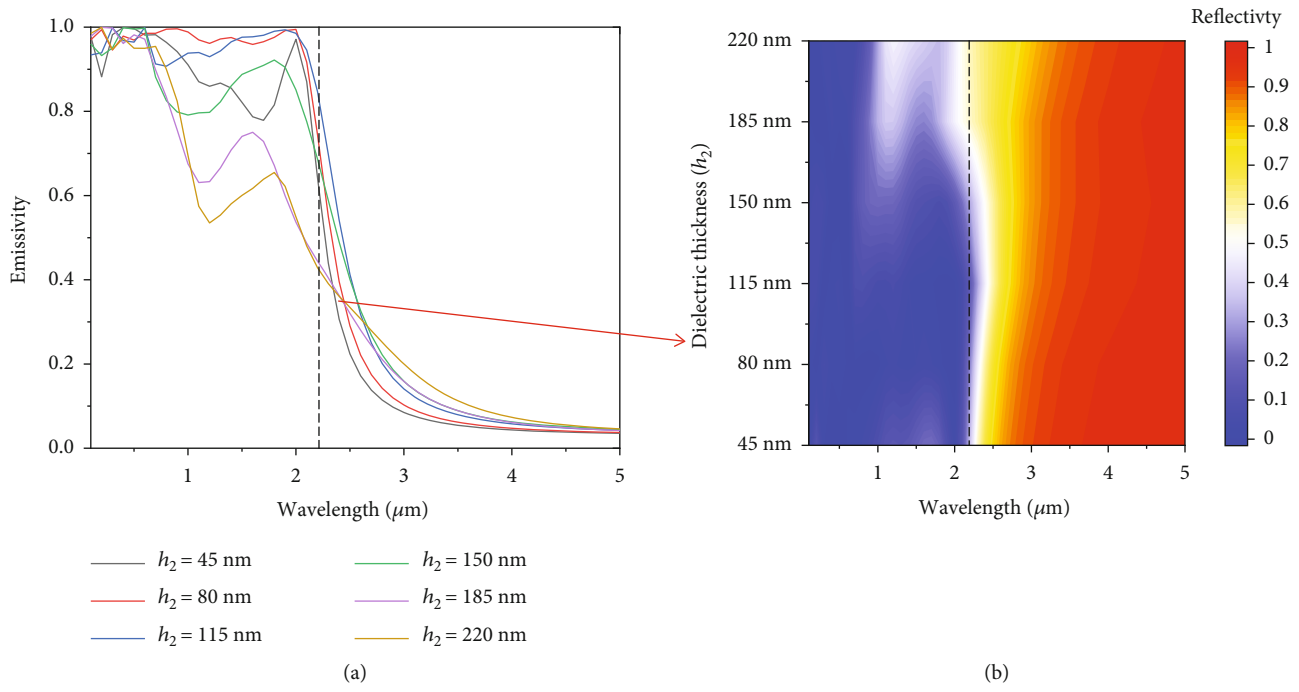

FIGURE 4: The effect of dielectric thickness (h_2) on the spectral (a) emissivity and (b) reflectivity of designed nanopyramid metamaterial with $b_1 = 215$ nm and $h_1 = 160$ nm.

nanopyramid TPV emitter. As seen in the graph, the AlN dielectric material has a high spectrum emissivity between 0.1 and 2.2 μm, and it declines at longer wavelengths.

Figures 7(d) and 7(e) compare the emissivity of produced nanopyramid metamaterials to those of thermal emitter metamaterials now in use. The shaded area represents InGaAs' external quantum efficiency (EQE). Due to its greater EQE before 2.2 m than the other cell, which has a 0.55 eV band gap energy [29], InGaAs was utilized as a TPV cell in this work. Figure 7(d) explains the emissivity of Wang et al.'s [21] nanopyramid gratings deposited on an ultrathin MgF_2 spacer and tungsten ground film by simulation (black line) and experimental (red line). As shown in this figure, the designed emitter has a high emissivity in the

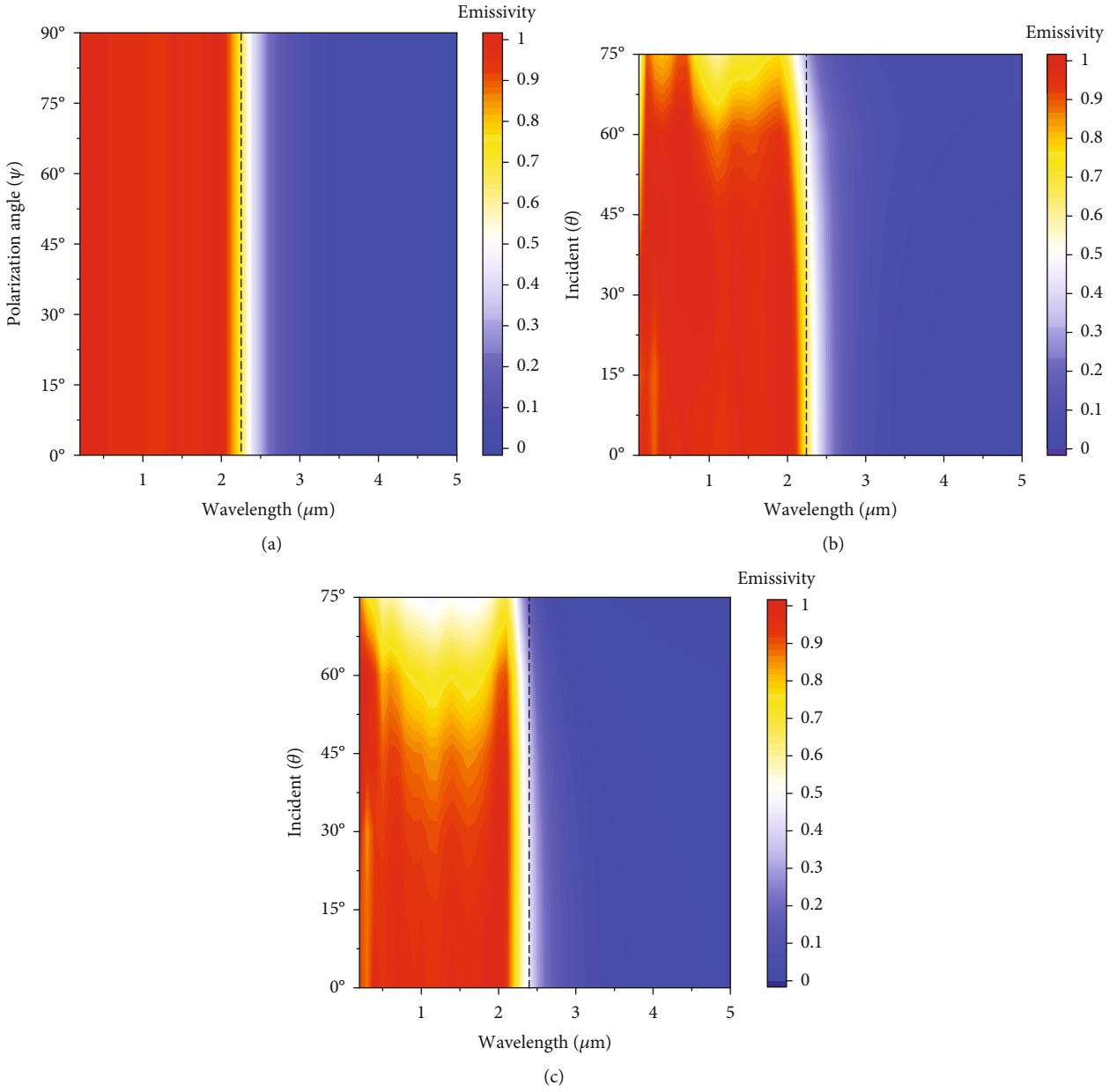

Figure 5: (a) The effect of polarization angle (ψ) on the spectral emissivity of designed nanopyramid MM emitter. (b) The effect of incident angle (θ) on the spectral emissivity of designed nanopyramid MM emitter for TM. (c) The effect of incident angle (θ) on the spectral emissivity of designed nanopyramid MM emitter for TE.

cutoff wavelength and a low emissivity above the cutoff wavelength compared to both the simulation result and the experimental result of Wang et al. [21], which have the same design as the designed emitter.

In Figure 7(e), the black line reflects Woolf et al. [30] and the red line indicates Maremi et al. [23], while the blue line displays the planned selective emitter emissivity. Figure 7(d) demonstrates how the emitter's broadband performance was almost flawless above the InGaAs band gap (shaded region or >2.2 μm) and substantially degraded below the InGaAs band gap (outside the shaded area or 2.2 μm). It was decided that radiation energy below the band gap in the TPV cell was waste energy and radiation energy above the band gap was necessary (convertible) energy. This result demonstrated that the planned emitter generated more highly convertible photons and covered a larger wavelength when compared to Woolf et al. [30] and Maremi et al. [23].

This work produced a nanopyramid metamaterial that enhances spectral efficiency in a TPV system. The effectiveness of the TPV system was examined in order to gauge the efficacy of an optimized emitter for a TPV cell. Equation (4) [23] provides the efficiency of a TPV system in converting radiated heat to electrical power.

$$\eta_{\mathrm{TPV}} = \eta_{\mathrm{SP}}\eta_{\mathrm{PV}} = \frac{P_{\mathrm{out}}}{P_{\mathrm{rad}}}, \tag{4}$$

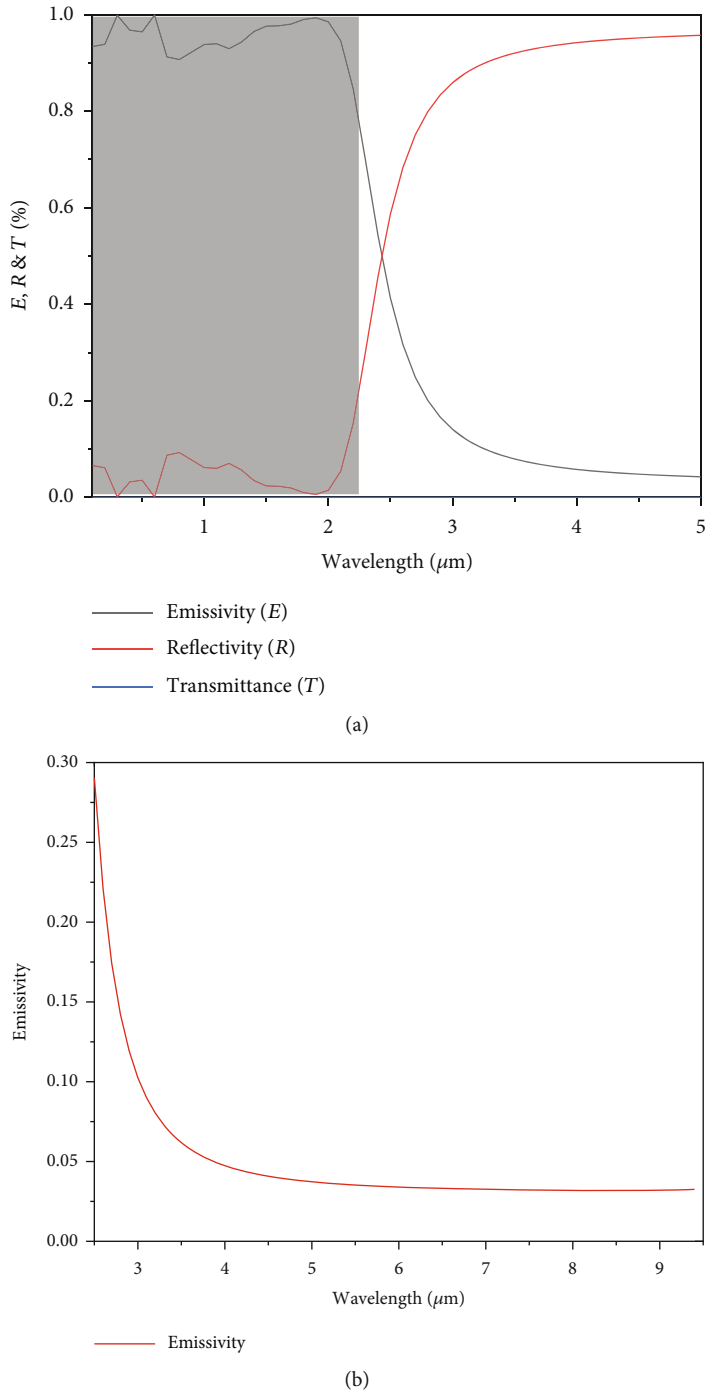

FIGURE 6: (a) Emissivity, reflectivity, and transmittance of the designed nanopyramid emitter with cutoff wavelength 2.2 μm. (b) The emissivity of nanopyramid emitter above 2.5 μm.

where η_{SP} is the spectral efficiency of the emitter, η_{PV} is the efficiency of the photovoltaic cell, P_{out} is the maximum output power, and P_{rad} is the total radiant power from an emitter. Spectral efficiency η_{SP} is defined by the following equation [23, 31]:

$$\eta_{SP} = \frac{\int_0^{\lambda_c} E(\lambda)\varepsilon(\lambda)d\lambda}{\int_0^{\infty} E(\lambda)\varepsilon(\lambda)d\lambda}, \quad (5)$$

$$E(\lambda) = \frac{2hc^2}{\lambda^5}\frac{1}{e^{(hc/\lambda KT)-1}}, \quad (6)$$

where λ_c is the cutoff wavelength, $E(\lambda)$ is the emission spectrum of a blackbody, K is the Boltzmann constant, h is Planck's constant, c is the medium's speed of light, and $\varepsilon(\lambda)$ is the spectral emissivity of the proposed selective emitter metamaterial.

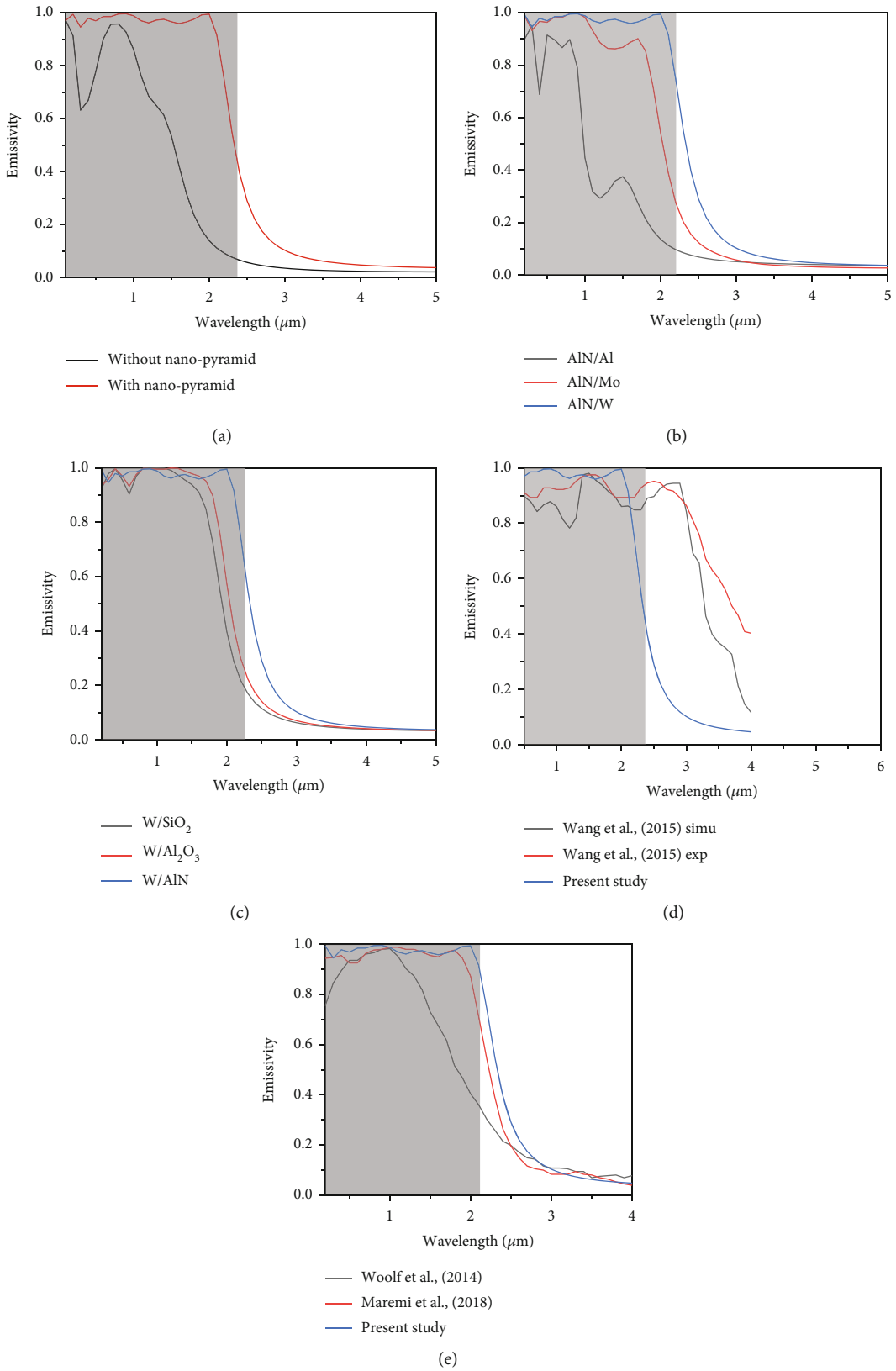

Figure 7: (a) The spectral emissivity of designed TPV emitter with and without nanopyramid. (b) The emittance spectra of the nanopyramid TPV emitter using AlN with different metal. (c) W with different dielectric material of the suggested TPV emitter. (d) The spectral emissivity of suggested emitter with simulation and experimental result of Wang et al. [21] for band gap of InGaAs. (e) The spectral emissivity of suggested emitter with Woolf et al. [30] and Maremi et al. [23] for EQE of InGaAs.

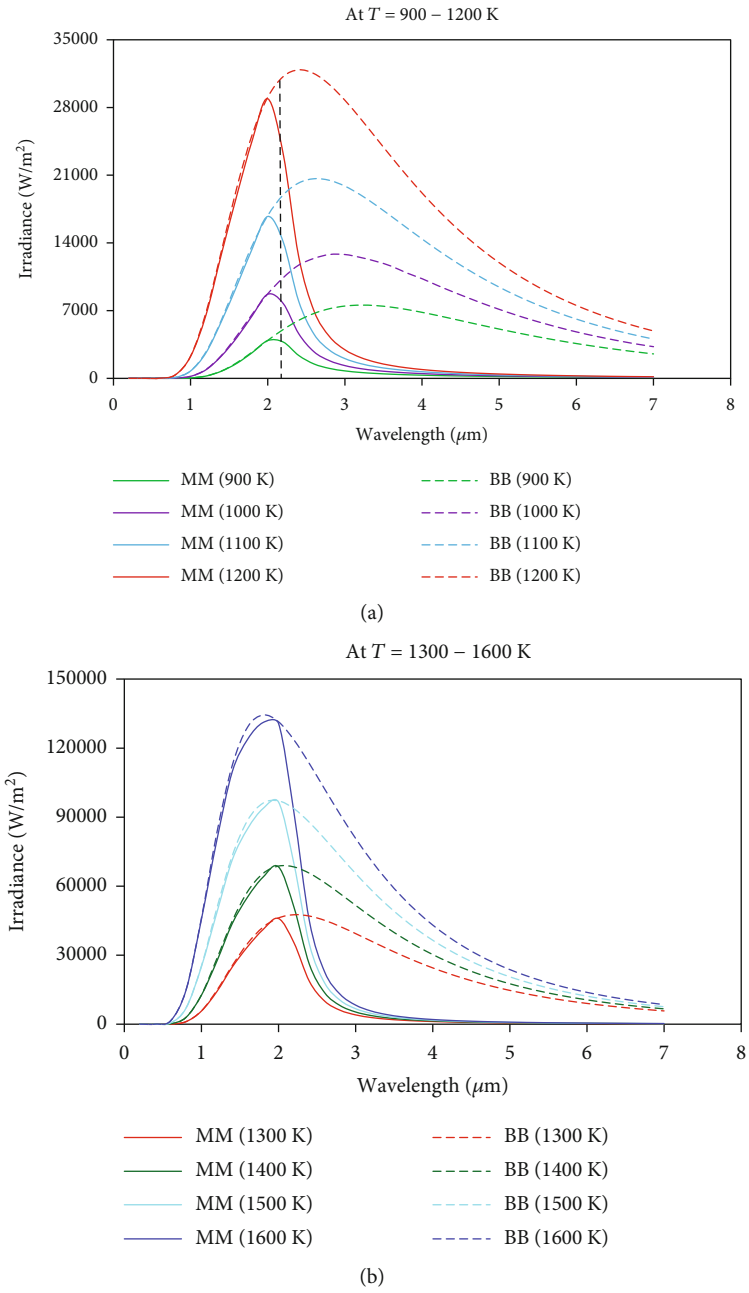

Figure 8: Comparison of the suggested emitter with the blackbody in terms of spectral emissivity at different temperatures.

The examination of the blackbody and the improved nanopyramid selective emitter's spectrum irradiance at temperatures 900 K to 1600 K is shown in Figures 8(a) and 8(b). The selective emitter works most effectively when its emissivity is excellent below the cutoff wavelength and poor above it. The emission peak was altered to a lower wavelength as the temperature rose, as predicted by Wien's law, and this suggested that the emission spectrum peak was above the band gap region. The spectral irradiance improved as the temperature rose. Before the cutoff wavelength, the optimized nanopyramid MM emitter had a high emissivity at $h_3 = 260$ nm, $w = 395$, $h_1 = 160$ nm, $h_2 = 80$ nm, and $b_1 = 215$ nm.

The graph in Figures 8(a) and 8(b) shows the emissivity of the proposed nanopyramid emitter as a solid line and the

Table 1: Spectral efficiency of designed emitter calculated at different temperatures.

Temperature	MM spectral efficiency
900 K	56%
1000 K	64%
1100 K	70.2%
1200 K	75%
1300 K	78.6%
1400 K	81.7%
1500 K	84%
1600 K	86.3%

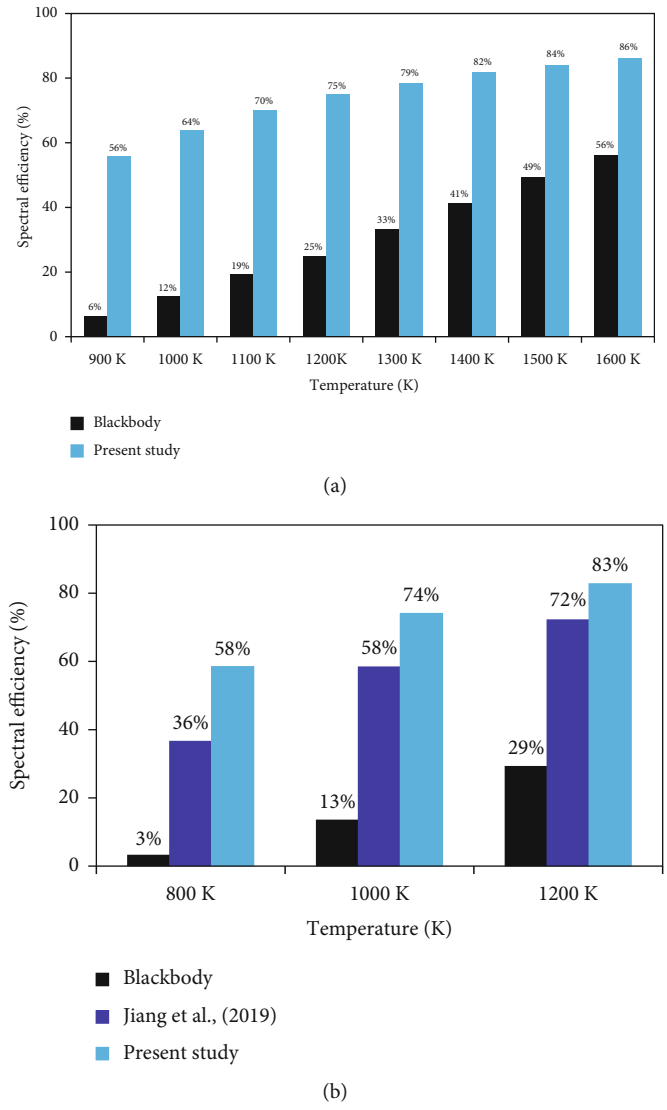

Figure 9: (a) Comparison of designed nanopyramid emitter spectral efficiency with blackbody spectral efficiency. (b) Comparison of the proposed nanopyramid metamaterial spectral efficiency with the spectral efficiency of blackbody and Jiang et al. [24] at 800 K, 1000 K, and 1200 K for EQE of InGaAsSb.

emissivity of the blackbody as a dotted line. Figures 8(a) and 8(b) compare the suggested emitter to the blackbody in terms of spectral emissivity at different temperatures and show the produced nanopyramid emitter's selective emission over the band gap. The cutoff wavelength of InGaAs, which is about 2.2 μm, is indicated by the vertical black dot line on both panels. The planned nanopyramid emitter had a lower spectral irradiance than the blackbody, which had a larger spectral irradiance above the cutoff wavelength (dotted line). This indicates that the emitter's emissions decreased the heating from waste spectrum irradiance that reached the TPV cell. The emitter was able to achieve great performance and a higher level of efficiency for the TPV system as a consequence.

Table 1 contains the spectral efficiency of the emitter at various temperatures that was determined using Equation (5). The results show that the spectral efficiency of the designed emitter was 78.6% and 84% at 1300 K and 1500 K, respectively, for the EQE of InGaAs, which was the highest, when compared to Smith et al. [27], who achieved spectral efficiency of 43% and 52%, and Maremi et al. [23], who achieved spectral efficiency of 76% and 82.4% at 1300 K and 1500 K, respectively. Excellent spectrum efficiency was necessary to increase the efficiency of TPV systems, as shown in Equation (4), and this study maximized the spectral efficiency more than the previous study. The spectral efficiency result was expressed as follows: when the temperature rose, the spectral efficiency of both the MM emitter and the blackbody increased. As a result, the spectral irradiance peak was moved to the left (to a shorter wavelength).

The spectral efficiency of a designed emitter and the blackbody is contrasted in Figure 9(a). The light blue histogram reflects the spectral efficiency of a constructed nanopyramid, whereas the black histogram represents the spectral efficiency of blackbody radiation. The nanopyramid

Table 2: Comparisons between the designed emitter and other emitters at room temperature.

	Materials		Geometry	Emissivity	Range of wavelength
	Metal	Dielectric			
Wang et al. [21]	W, Ti	MF_2	Pyramid	0.925	500-2200 nm
Song et al. [25]	W	SiO_2	2D rectangular	0.801	200-2200 nm
Maremi et al. [23]	W	AlN	Multilayer Ring	0.938	200-2200 nm
Jiang et al. [24]	W	Al_2O_3	Multilayer ring	0.943	500-2200 nm
Abdel-Latif et al. [7]	W	SiO_2	2D cylindrical gear	0.853	300-2200 nm
Present study	W	AlN	Pyramid	0.964	100-2200 nm

MM emitter has a better spectral efficiency than the blackbody, as seen in the picture. This demonstrates that the planned emitter could convert more radiation than the blackbody. In contrast, the designed nanopyramid metamaterial converted 75% of the energy radiated at a temperature similar to that of the blackbody, demonstrating that at 1200 K, the suggested emitter increased the TPV system's efficiency threefold. The picture also shows that the spectral efficiency of the blackbody and the purported emitter grew considerably with temperature.

Figure 9(b) shows a comparison of the proposed nanopyramid metamaterial spectral efficiency with the spectral efficiency of a blackbody and Jiang et al. [24] at 800 K, 1000 K, and 1200 K. The image shows the spectral efficiency of the blackbody and a multilayer MM emitter for EQE of InGaAsSb at 800 K, 1000 K, and 1200 K. The black and blue histograms in the picture depict the spectral efficiency of the blackbody and a multilayer MM emitter for EQE of InGaAsSb at 800 K, 1000 K, and 1200 K, respectively, whereas the light blue histogram shows the spectral efficiency of the designed metamaterial for EQE of InGaAsSb. As shown in the figure, the blackbody converts 3%, 13%, and 29% of radiated energies at 800 K, 1000 K, and 1200 K, respectively, and the multilayer ring of Jiang et al. [24] converts 36.4%, 58%, and 72% of radiated energy at similar temperatures for the EQE of InGaAsSb. However, the designed emitter converts about 58%, 74%, and 83% of the radiated energy at 800 K, 1000 K, and 1200 K, respectively, for the EQE of InGaAsSb. This finding indicates that designed nanopyramid emitters convert more energy than blackbodies and Jiang et al. [24].

The developed nanopyramid emitter is compared to various metamaterials in relation to emitters' materials and emissivity in Table 2. The recommended emitter outperformed those listed in Table 2 by achieving a high emissivity of around 0.964 over a broad spectrum of wavelengths from 0.1 μm to 2.2 μm. Further, different scholars have designed metamaterial emitters with different materials and geometry. Shoaei [29], for example, designed a pyramid nanostructure emitter with tungsten as the bottom metal, magnesium fluoride (MF_2) as a dielectric spacer, and titanium (Ti) at the top. Woolf et al. [30] designed 2D trilayer films, Maremi et al. [23] created a multilayer ring geometry grating from W and AlN, Jiang et al. [24] created a multilayer ring geometry grating from W and SiO_2, and Abdel-Latif et al. [7] created a 2D cylindrical gear grating from W and SiO_2. Their emissivity and the range of wavelengths they absorb are given in the table below.

4. Conclusion

A wavelength-selective TPV emitter based on a nanopyramid made of tungsten and aluminum nitride dielectric spaces with a cutoff wavelength match to InGaAs with an energy band gap of 0.55 eV was studied numerically. The geometrical factors along the wavelength have a significant influence on the spectral emissivity of the proposed TPV emitter. In order to maximize the estimated emissivity, the effects of the pyramid's base length (b_1), height (h_1), and dielectric thickness (h_2) were researched. The proposed metamaterial increased the efficiency of the TPV system. The suggested metamaterial emitter demonstrated a nearly perfect broadband and average wide-angle emissivity of over 96% attained between the wavelengths of 0.1 μm and 2.2 μm when the period $(w) = 395$ nm, $h_3 = 260$ nm, $h_1 = 160$ nm, $h_2 = 80$ nm, and $b_1 = 215$ nm. The emissivity, however, decreased sharply to less than 5% behind 2.2 μm. This outcome demonstrates an increase in the emitter's spectral efficiency. A wide variety of incidence angles from 0° to 60° were supported by the developed metamaterial emitter, which demonstrated polarization independence and produced excellent emissivity. Also, the developed emitter outperformed the blackbody in terms of spectral efficiency for the InGaAs TPV cell and for both the blackbody and Jiang et al. [24] for the InGaAsSb TPV cell. Finally, the spectral efficiency of the designed metamaterial emitter for the InGaAs TPV cell was around 75% at 1200 K and 86.2% at 1600 K, respectively. This exemplifies how crucial the emitter's design is to enhancing the TPV system's effectiveness and performance.

Data Availability

The data used to support the findings of this study are available from the corresponding author upon request.

Conflicts of Interest

The authors declare that they have no conflicts of interest.

Authors' Contributions

All authors contributed to the study's conception and design. The processes of conceptualizing, designing, data analysis, and interpretation were performed by all authors (Gurmu Alemu, Sifan Tamiru, Fekadu Tolessa, Soloman Tiruneh, Abebe Belay, and Gurumurthi Thillainayagam).

The first draft of the manuscript was written by Sifan Tamiru, and all authors commented on previous versions of the manuscript. All authors read and approved the final manuscript after critical revision. All authors met the requirements for authorship, and they confirm that the manuscript represents honest work.

Acknowledgments

This study was supported by the Adama Science and Technology University, Adama, Ethiopia.

References

[1] D. Chubb, *Fundamentals of Thermophotovoltaic Energy Conversion*, Elsevier, 2007.

[2] N. A. Pfiester and T. E. Vandervelde, "Selective emitters for thermophotovoltaic applications," *Physica Status Solidi*, vol. 214, no. 1, article 1600410, 2017.

[3] S. G. Babiker, S. Yong, M. O. Sid-Ahmed, and X. Ming, "Thermophotovoltaic emitters based on a one-dimensional metallic-dielectric multilayer nanostructures," *Journal of Electronics Cooling and Thermal Control*, vol. 4, no. 1, pp. 39–48, 2014.

[4] M. M. A. Gamel, H. J. Lee, W. E. S. W. A. Rashid et al., "A review on thermophotovoltaic cell and its applications in energy Conversion: Issues and Recommendations," *Issues and Recommendations Materials*, vol. 14, no. 17, p. 4944, 2021.

[5] D. N. Woolf, E. A. Kadlec, D. Bethke et al., "High-efficiency thermophotovoltaic energy conversion enabled by a metamaterial selective emitter," *Optica*, vol. 5, no. 2, pp. 213–218, 2018.

[6] H. Wang, J. Y. Chang, Y. Yang, and L. Wang, "Performance analysis of solar thermophotovoltaic conversion enhanced by selective metamaterial absorbers and emitters," *International Journal of Heat and Mass Transfer, vo*, vol. 98, no. 98, pp. 788–798, 2016.

[7] G. Y. Abdel-Latif, M. F. O. Hameed, and S. S. A. Obayya, "Characteristics of thermophotovoltaic emitter based on 2D cylindrical gear grating," *Optical and Quantum Electronics*, vol. 53, no. 3, pp. 1–14, 2021.

[8] S. Basu, Y. B. Chen, and Z. M. Zhang, "Microscale radiation in thermophotovoltaic devices a review," *International Journal of Energy Research*, vol. 31, no. 6-7, pp. 689–716, 2007.

[9] W. Gu, G. Tang, and W. Tao, "High efficiency thermophotovoltaic emitter by metamaterial-based nano-pyramid array," *Optics Express*, vol. 23, no. 24, pp. 30681–30694, 2015.

[10] R. Sakakibara, V. Stelmakh, W. R. Chan et al., "Practical emitters for thermophotovoltaics: a review," *Journal of Photonics for Energy*, vol. 9, pp. 032713–032713, 2019.

[11] C. Ferrari, F. Melino, M. Pinelli, P. R. Spina, and M. Venturini, "Overview and status of thermophotovoltaic systems," *Energy Procedia*, vol. 45, pp. 160–169, 2014.

[12] E. Nefzaoui, J. Drevillon, and K. Joulain, "Selective emitters design and optimization for thermophotovoltaic applications," *Journal of Applied Physics*, vol. 111, no. 8, article 084316, 2012.

[13] B. Bitnar, W. Durisch, J. C. Mayor, H. Sigg, and H. R. Tschudi, "Characterisation of rare earth selective emitters for thermophotovoltaic applications," *Solar Energy Materials and Solar Cells*, vol. 73, no. 3, pp. 221–234, 2002.

[14] S. Y. Lin, J. Moreno, and J. G. Fleming, "Three-dimensional photonic-crystal emitter for thermal photovoltaic power generation," *Applied Physics Letters*, vol. 83, no. 2, pp. 380–382, 2003.

[15] R. A. Shelby, D. R. Smith, and S. Schultz, "Experimental verification of a negative index of refraction," *Science*, vol. 292, no. 5514, pp. 77–79, 2001.

[16] A. Valipour, M. H. Kargozarfard, M. Rakhshi, A. Yaghootian, and H. M. Sedighi, "Metamaterials and their applications: an overview," *Proceedings of the Institution of Mechanical Engineers, Part L: Journal of Materials: Design and Applications*, vol. 236, no. 11, pp. 2171–2210, 2022.

[17] N. I. Landy, S. Sajuyigbe, J. J. Mock, D. R. Smith, and W. J. Padilla, "Perfect metamaterial absorber," *Physical Review Letters*, vol. 100, no. 20, article 207402, 2008.

[18] G. R. Fowles, *Introduction to Modern Optics*, Courier Corporation, 1989.

[19] C. Shemelya, D. DeMeo, N. P. Latham et al., "Stable high temperature metamaterial emitters for thermophotovoltaic applications," *Applied Physics Letters*, vol. 104, no. 20, article 201113, 2014.

[20] H. Wang, Q. Chen, L. Wen, S. Song, X. Hu, and G. Xu, "Titanium-nitride-based integrated plasmonic absorber/emitter for solar thermophotovoltaic application," *Photonics Research*, vol. 3, no. 6, pp. 329–334, 2015.

[21] H. Wang, V. Prasad Sivan, A. Mitchell, G. Rosengarten, P. Phelan, and L. Wang, "Highly efficient selective metamaterial absorber for high-temperature solar thermal energy harvesting," *Solar Energy Materials and Solar Cells*, vol. 137, pp. 235–242, 2015.

[22] Y. Da and Y. Xuan, "Perfect solar absorber based on nanocone structured surface for high-efficiency solar thermoelectric generators," *Science China Technological Sciences*, vol. 58, no. 1, pp. 19–28, 2015.

[23] F. T. Maremi, N. Lee, G. Choi, T. Kim, and H. H. Cho, "Design of multilayer ring emitter based on metamaterial for thermophotovoltaic applications," *Energies*, vol. 11, no. 9, p. 2299, 2018.

[24] C. Jiang, S. Shan, Z. Zhou, L. Liang, and H. Huang, "Theoretical study of multilayer ring metamaterial emitter for a low bandgap TPV cell," *Solar Energy*, vol. 194, pp. 548–553, 2019.

[25] J. Song, M. Si, Q. Cheng, and Z. Luo, "Two-dimensional trilayer grating with a metal/insulator/metal structure as a thermophotovoltaic emitter," *Applied Optics*, vol. 55, no. 6, pp. 1284–1290, 2016.

[26] G. Y. Abdelatif, M. F. Hameed, S. S. Obayya, and M. Hussein, "Ultrabroadband absorber based on a funnel-shaped anisotropic metamaterial," *JOSA B*, vol. 36, no. 10, pp. 2889–2895, 2019.

[27] D. Y. Smith, E. Shiles, M. Inokuti, and E. Palik, "The optical properties of metallic aluminum," in *Handbook of Optical Constants of Solid*, pp. 369–406, Academic Press, 1985.

[28] H. Lee, T. Kim, M. F. Tolessa, and H. H. Cho, "Enhancing radiative cooling performance using metal-dielectric-metal metamaterials," *Journal of Mechanical Science and Technology*, vol. 31, no. 11, pp. 5107–5112, 2017.

[29] E. Shoaei, "Performance assessment of thermophotovoltaic application in steel industry," *Solar Energy Materials and Solar Cells*, vol. 157, pp. 55–64, 2016.

[30] D. Woolf, J. Hensley, J. G. Cederberg, D. T. Bethke, A. D. Grine, and E. A. Shaner, "Heterogeneous metasurface for high temperature selective emission," *Applied Physics Letters*, vol. 105, no. 8, article 081110, 2014.

[31] V. Rinnerbauer, A. Lenert, D. M. Bierman et al., "Metallic photonic crystal Absorber-Emitter for efficient spectral control in High-Temperature solar thermophotovoltaics," *Advanced Energy Materials*, vol. 4, no. 12, article 1400334, 2014.